Applied Mathematics Letters 114 (2021) 106918

Contents lists available at ScienceDirect

Applied Mathematics Letters

www.elsevier.com/locate/aml

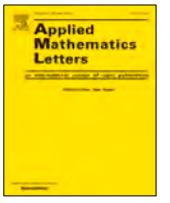

Exact sharp-fronted travelling wave solutions of the Fisher–KPP equation

Scott W. McCue *, Maud El-Hachem, Matthew J. Simpson

School of Mathematical Sciences, Queensland University of Technology, Brisbane, Australia

ARTICLE INFO

Article history:
Received 1 September 2020
Received in revised form 22 November 2020
Accepted 22 November 2020
Available online 30 November 2020

Keywords:
Fisher–Kolmogorov
Painlevé property
Weierstraß elliptic functions
Moving boundary problem

ABSTRACT

A family of travelling wave solutions to the Fisher–KPP equation with speeds $c = \pm 5/\sqrt{6}$ can be expressed exactly using Weierstraß elliptic functions. The well-known solution for $c = 5/\sqrt{6}$, which decays to zero in the far-field, is exceptional in the sense that it can be written simply in terms of an exponential function. This solution has the property that the phase-plane trajectory is a heteroclinic orbit beginning at a saddle point and ending at the origin. For $c = -5/\sqrt{6}$, there is also a trajectory that begins at the saddle point, but this solution is normally disregarded as being unphysical as it blows up for finite z. We reinterpret this special trajectory as an exact sharp-fronted travelling solution to a *Fisher–Stefan* type moving boundary problem, where the population is receding from, instead of advancing into, an empty space. By simulating the full moving boundary problem numerically, we demonstrate how time-dependent solutions evolve to this exact travelling solution for large time. The relevance of such receding travelling waves to mathematical models for cell migration and cell proliferation is also discussed.

1. Introduction

For various applications in ecology and cell biology, the Fisher–KPP equation [1–3]

$$\frac{\partial u}{\partial t} = \frac{\partial^2 u}{\partial x^2} + u(1-u), \tag{1}$$

provides a very well studied model for the growth and spread of a population of species or cell types [4–6]. One key mathematical result is that, with the associated initial and boundary conditions

$$u(x,0) = F(x), \quad 0 < x < \infty, \tag{2}$$

$$\frac{\partial u}{\partial x} = 0 \quad \text{on} \quad x = 0, \quad u \to 0 \quad \text{as} \quad x \to \infty, \tag{3}$$

* Corresponding author.
E-mail address: scott.mccue@qut.edu.au (S.W. McCue).

https://doi.org/10.1016/j.aml.2020.106918
0893-9659/

the time-dependent solution evolves towards a travelling wave profile $U(z)$, where $z = x - ct$, as $t \to \infty$ [1–3]. A combination of phase-plane analysis and simple asymptotics demonstrates that the travelling wave speed c satisfies $c \geq 2$ and is selected by the far-field behaviour of the initial condition $F(x)$ in (2) [4–6].

In this work, we are motivated by our recent studies [7–10] where we have restricted the Fisher–KPP equation (1) to hold on the moving domain $0 < x < s(t)$, together with a Stefan-type moving boundary condition, to give the so-called *Fisher–Stefan* model [11]

$$\frac{\partial u}{\partial t} = \frac{\partial^2 u}{\partial x^2} + u(1-u), \quad 0 < x < s(t), \tag{4}$$

$$\frac{\partial u}{\partial x} = 0 \quad \text{on} \quad x = 0, \tag{5}$$

$$u = 0, \quad \frac{\mathrm{d}s}{\mathrm{d}t} = -\kappa \frac{\partial u}{\partial x} \quad \text{on} \quad x = s(t). \tag{6}$$

Here κ is a parameter that relates the leakage of the population at the boundary to the speed of the boundary. Note that the second condition in (6) is required because we are dealing with a moving boundary problem and so there is an additional degree freedom for the moving boundary $x = s(t)$ when compared to a fixed boundary. We choose this precise form as it is the most straightforward way to relate the speed of the interface to the population flux, but also because of the direct analogy with Stefan-type moving boundary problems (heat conduction problems accompanied by a change of phase) [12–14].

In the context of (4)–(6), we and others have provided new interpretations for travelling wave solutions (1) for $c < 2$, including slowly moving fronts that advance with speed $0 < c < 2$ (these are for $\kappa > 0$, with $c \to 2^-$ as $\kappa \to \infty$) [7,11,15–17], stationary profiles for $c = 0$ ($\kappa = 0$) and receding fronts with speed $c < 0$ (here $-1 < \kappa < 0$, with $c \to -\infty$ as $\kappa \to -1^+$) [8,10]. Travelling wave solutions for $c < 2$ are interesting because they are normally disregarded as being unphysical (since they do not satisfy the boundary conditions and/or are not restricted to $0 < U < 1$ for all $z \in \mathbb{R}$) [1–6].

In this letter we focus on travelling wave solutions to (1) for the special values $c = \pm 5/\sqrt{6}$. For $c = 5/\sqrt{6}$ there is a well known exact solution [4,18]

$$U = \left(1 + (\sqrt{5} - 1)\, \mathrm{e}^{z/\sqrt{6}}\right)^{-2}, \tag{7}$$

as shown in Fig. 1(a)–(b). Other exact travelling wave solutions to (1) for $c = \pm 5/\sqrt{6}$, which can be written in terms of Weierstraß elliptic functions [19], are normally disregarded as being unphysical in the usual way [4]. However, in the context of the Fisher–Stefan model (4)–(6), we provide a new physical interpretation of one of these solutions. In particular, we claim that one of the profiles for $c = -5/\sqrt{6}$ corresponds to a receding travelling wave to (4)–(5) with a special value of $\kappa = -0.906\ldots$. In this way, we illustrate a second physically realistic exact travelling wave solution to (1) for $c = \pm 5/\sqrt{6}$.

In Section 2 we review the exact travelling solutions to the Fisher–KPP equation for $c = \pm 5/\sqrt{6}$, taken from Ablowitz & Zeppetella [19]. This derivation involves elliptic functions and, in particular, the equianharmonic case of the Weierstraß p-function [20]. By using phase-plane analysis, we demonstrate the qualitative behaviour of this family of solutions and highlight the two special trajectories that evolve to $(U, V) = (1, 0)$ as $z \to -\infty$. In Section 3 we link this special trajectory to solutions of the Fisher–Stefan model and demonstrate numerically that for $\kappa = -0.906\ldots$, initial conditions evolve to this travelling wave solution for large time. Finally, we provide concluding remarks in Section 4.

2. Travelling wave solutions for $c = \pm 5/\sqrt{6}$

To study travelling wave solutions of (1) we write $u = U(z)$, where $z = x - ct$, to give

$$\frac{\mathrm{d}^2 U}{\mathrm{d}z^2} + c\frac{\mathrm{d}U}{\mathrm{d}z} + U(1-U) = 0. \tag{8}$$

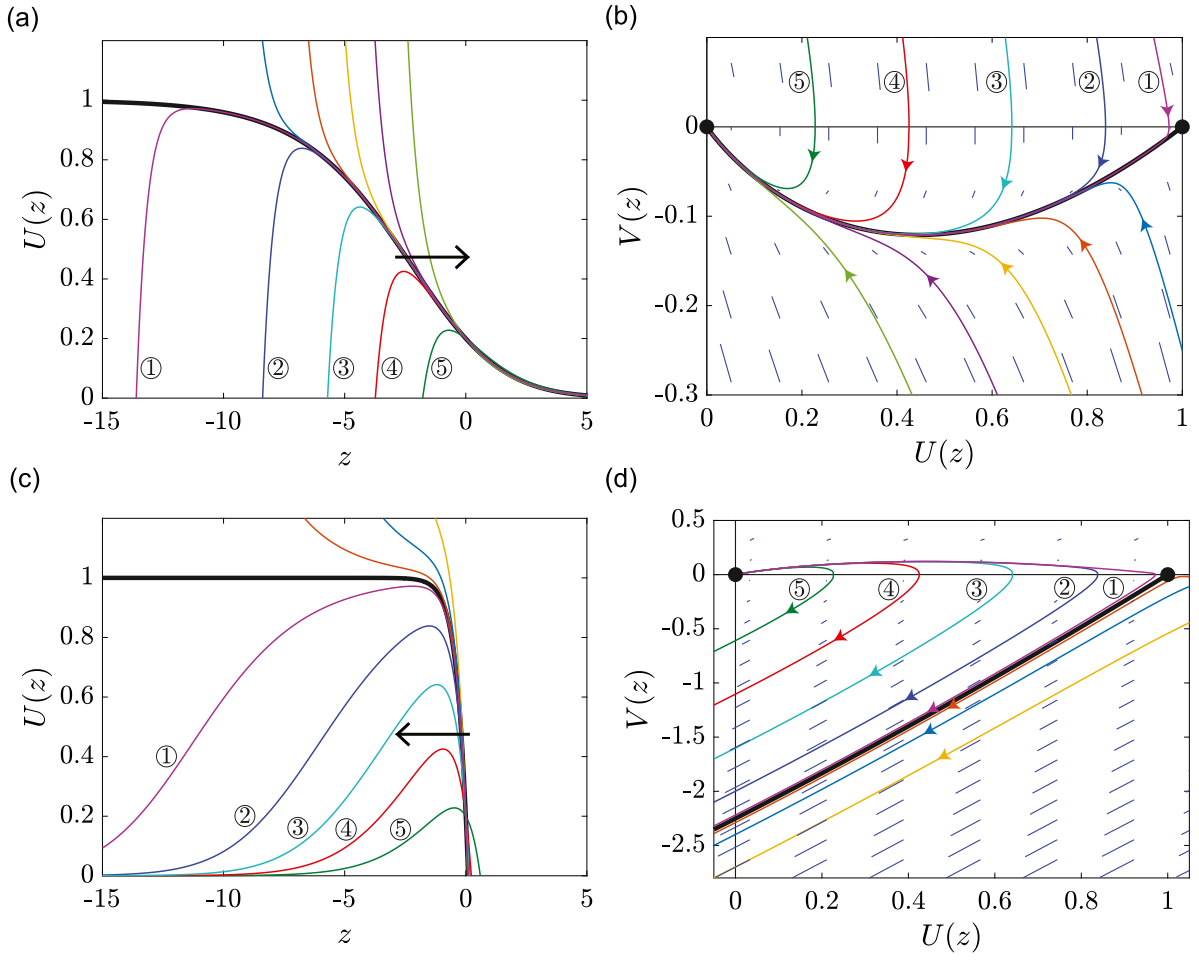

Fig. 1. Exact solutions to the Fisher–KPP model. (a)–(b) shows the exact solutions for $c = 5/\sqrt{6}$ in the physical plane and the phase plane, respectively. Similarly, (c)–(d) shows the exact solutions for $c = -5/\sqrt{6}$ in the physical plane and the phase plane, respectively. (a), (c) show the travelling wave profiles $U(z)$ that satisfy (13), with horizontal arrows superimposed to emphasise the difference in direction. (b), (d) show various phase plane trajectories, with equilibrium points in the phase planes shown with black discs. Solutions and trajectories corresponding to the physically relevant boundary condition (9) are plotted in thick black curves. Various other trajectories (thin coloured lines) are superimposed, and the corresponding curves are given in (a),(c) using the same colours as in (b), (d). Some trajectories are numbered to emphasise the point that the numbered trajectories in (a)–(d) are identical. (For interpretation of the references to colour in this figure legend, the reader is referred to the web version of this article.)

We discuss the domain of interest and the boundary conditions below, but for the moment we highlight the physically relevant boundary condition

$$U \to 1^-, \quad \frac{\mathrm{d}U}{\mathrm{d}z} \to 0^-, \quad \text{as} \quad z \to -\infty, \tag{9}$$

which applies for two special cases considered below. We rewrite (8) in the usual way as

$$\frac{\mathrm{d}U}{\mathrm{d}z} = V, \tag{10}$$

$$\frac{\mathrm{d}V}{\mathrm{d}z} = -cV - U(1-U). \tag{11}$$

One point to note here is that this system is reversible under the substitution $z \to -z$, $V \to -V$, $c \to -c$, which means that the phase-plane for (10)–(11) for $c < 0$ is simply a reflection about the U-axis of the phase-plane for $c > 0$.

The concern here is with the special values $c = \pm 5/\sqrt{6}$. For these values, we may solve (8) exactly, as explained by Ablowitz & Zeppetella [19]. A summary of the working is as follows. We start by letting $U = f(z)w(z)$ and substituting into (8). Then, by forcing $f'' + cf' + f = 0$, we find $fw'' + (2f' + cf)w' = f^2 w^2$. Choose the linearly independent solution $f = \mathrm{e}^{\lambda z}$, where $\lambda = (-c + \sqrt{c^2 - 4})/2$, so that $w'' + \sqrt{c^2 - 4}w' = \mathrm{e}^{\lambda z} w^2$. The equations simplify by setting $w = w(s)$, $s = h(z)$. The left-hand side of this differential equation reduces to a single term if $h'' + \sqrt{c^2 - 4}h' = 0$, which suggests we choose $h = \mathrm{e}^{-\sqrt{c^2-4}z}$. Finally, with $c^2 = 25/6$ we end up with the second-order differential equation for w to be $\mathrm{d}^2 w/\mathrm{d}s^2 = 6w$ which, upon multiplying both sides by $\mathrm{d}w/\mathrm{d}s$, integrates directly to

$$\left(\frac{\mathrm{d}w}{\mathrm{d}s}\right)^2 = 4w^3 - g_3, \tag{12}$$

where g_3 is a constant (often referred to as an elliptic invariant). The first-order ode (12) is separable and is solved exactly in terms of the Weierstraß p-function $\wp(z; 0; g_3)$ [20]. Rewriting the solution in terms of U and V gives

$$U = \mathrm{e}^{-2z/\sqrt{6}} \wp\left(\mathrm{e}^{-z/\sqrt{6}} - k; 0; g_3\right), \tag{13}$$

$$V = -\frac{\sqrt{6}}{3}\mathrm{e}^{-2z/\sqrt{6}} \left(\wp\left(\mathrm{e}^{-z/\sqrt{6}} - k; 0; g_3\right) + 2\mathrm{e}^{-z/\sqrt{6}} \wp'\left(\mathrm{e}^{-z/\sqrt{6}} - k; 0; g_3\right)\right), \tag{14}$$

where $\wp'$ is the derivative of $\wp$ [20] and k is a constant of integration. It is noteworthy that this exact solution is possible because (8) has the Painlevé property for $c = \pm 5/\sqrt{6}$. In other words, for these special values of c, the movable singularities of solutions to (8) are poles [21].

We shall use the following important properties of the Weierstraß p-function. Since the second argument of $\wp$ (the elliptic invariant which is often denoted as g_2) is zero, we can apply the scaling transformation $\wp(\zeta; 0; g_3) = \mu^2 \wp(\mu\zeta; 0, g_3/\mu^6)$ to relate our exact solution (13) to the so-called equianharmonic case $\wp(\zeta; 0; 1)$, which has a double pole at the origin. The special case $\wp(\zeta; 0; 1)$ is real, positive and periodic along the real axis with period $2\omega_2$, where

$$\omega_2 = \frac{\Gamma^3(1/3)}{4\pi} \tag{15}$$

is one of the generators and $\Gamma(z)$ is the gamma function [20]. This is useful for the cases in which $g_3 > 0$. Further, $\wp(\zeta; 0; 1)$ is real and periodic up the imaginary axis with period $2\sqrt{3}\omega_2$ ($= 4\omega_1 + 2\omega_2$, where ω_1 is the other generator). These properties are useful for $g_3 < 0$.

It is worth plotting the exact solutions (13)–(14) both in the form $U = U(z)$ and in the phase-plane. As the travelling wave solutions are invariant to translations in z, we fix each solution in the z-direction by setting $U = U_0$ at $z = 0$. For a given point in the phase plane, $(U, V) = (U_0, V_0)$, we determine the two constants k and g_3 by solving the nonlinear algebraic system $U_0 = \wp(1 - k; 0; g_3)$, $V_0 = -(\sqrt{6}/3)\left(\wp(1 - k; 0; g_3) + 2\wp'(1 - k; 0; g_3)\right)$ numerically, for example with Newton's method. Note that the periodic nature of $\wp$ means that there are infinitely many combinations of g_3 and k that satisfy these algebraic equations; any of these combinations will give the same solution for (U, V).

Fixing $c = 5/\sqrt{6}$ for the moment, travelling wave profiles $U(z)$ are shown in Fig. 1(a), while corresponding trajectories in the phase-plane are shown in Fig. 1(b). Each of these curves could be drawn using the exact solution (13)–(14) or just as easily be generated using numerical solutions to (10)–(11). As is well known, the phase-plane in Fig. 1(b) is characterised by two fixed points, namely the saddle point at $(1, 0)$ and the stable node at $(0, 0)$. All of the trajectories in Fig. 1(b) enter the stable node $(0, 0)$; a linearisation about $(0, 0)$ demonstrates that $U \sim \text{const}\, \mathrm{e}^{-2z/\sqrt{6}}$ as $z \to \infty$. As z decreases, we see in both Fig. 1(a) and (b) that, with one exception, each solution (thin coloured curves) blows up (with $U \to \pm\infty$) at a finite value of z. For the solutions that remain positive for all z ($U > 0$), the constant $g_3 > 0$, and so the value of z

at which U blows up, z_∞ say, occurs when $g_3^{1/6}(\mathrm{e}^{-z_\infty/\sqrt{6}} - k)$ approaches the closest value of $2n\omega_2$, for a positive integer n, where ω_2 is given by (15). That is, $z_\infty = -\sqrt{6}\ln(2n\omega_2/g_3^{1/6} + k)$. For the solutions which intersect the U-axis ($U < 0$ for certain intervals in z), $g_3 < 0$; in these cases the solution blows up when $z_\infty = -\sqrt{6}\ln(2\sqrt{3}m\omega_2/(-g_3)^{1/6} + k)$, for a positive integer m. The exception is the heteroclinic orbit (thick black curve) that joins the two fixed points; this trajectory corresponds to the well-known exact solution (7), which notably satisfies the physically realistic boundary condition (9). The simplification from (13)–(14) to (7) in this case arises because this special case corresponds to taking the limit $g_3 \to 0$, which is in effect *pushing* the singularity to $z = -\infty$. Numerical solutions to (1)–(3) with appropriate initial conditions evolve to (7), as we demonstrate in Section 3.

Now turning to $c = -5/\sqrt{6}$, we show results in Fig. 1(c)–(d). Here it is convenient to reflect our phase-plane about the U-axis, so the heteroclinic orbit just mentioned is in the upper-half plane. The trajectories in the phase-plane are still given by (13)–(14), except that we must make the changes $V \to -V$, $z \to -z$. Five of the solutions shown in Fig. 1(c)–(d) are the same as in Fig. 1(a)–(b) (to enable a straightforward comparison across the figures, we have labelled these solutions ①–⑤); these are trajectories that start at the stable node $(0, 0)$, except now we see that $U \sim \text{const}\,\mathrm{e}^{2z/\sqrt{6}}$ as $z \to -\infty$. As we follow these trajectories for increasing z, we again note that they blow up at a finite value of z (with $U \to -\infty$ as $z \to -z_\infty^-$, remembering that we have reflected z in Fig. 1(c)–(d)). Other trajectories also blow up for finite z (this time with $U \to \infty$), except for the separatrix (solid black curve) which eventually enters the saddle point $(1, 0)$.

We now interpret the separatrix in Fig. 1(d) in terms of an exact sharp-fronted travelling wave solution of (1). As explained in Ablowitz & Zeppetella [19], in order to extract this special case from (13)–(14), we must choose the constants k and g_3 such that $\wp(\zeta; 0, g_3)$ has one of its double poles at $\zeta = -k$. Or, in other words, provided $g_3 > 0$, then $-kg_3^{1/6} = 2n\omega_2$ for a positive integer n, where ω_2 is defined by (15). That is, we require the numerical constraint

$$U_0 = \wp(1 + 2n\omega_2/g_3^{1/6}; 0; g_3), \tag{16}$$

where $0 < U_0 < 1$ (if $g_3 < 0$ the condition is $-k(-g_3)^{1/6} = 2\sqrt{3}m\omega_2$ for a positive integer m and so this constraint can be replaced by $U_0 = \wp(1 + 2\sqrt{3}m\omega_2/(-g_3)^{1/6}; 0; g_3)$). In Fig. 1(c) we have chosen $U_0 = 0.2$, but of course this value is arbitrary and, in effect, corresponds to a translation in z. The key observation of this special solution is that it satisfies the physically realistic boundary condition (9) as $z \to -\infty$. As we see in Fig. 1(c), as z increases, this solution for U is very flat until it decreases sharply to $U = 0$ at some finite value of $z = z^*$ where $V = V^* = -2.25\ldots$, and then continues to decrease as z increases further. While this solution satisfies (9), it is normally disregarded as it is negative for all $z > z_c$. In the following section we show how this profile is a receding travelling wave solution for the Fisher–Stefan moving boundary problem (4)–(6).

We close this section by noting that it is possible to use the exact solutions for $c = \pm 5/\sqrt{6}$ as the first term in a perturbation expansion valid for $c \mp 5/\sqrt{6} \ll 1$, with a view to deriving analytical approximations for a range of c values (including the case $c = 2$, which is very close to $c = 5/\sqrt{6}$). However, the linear system for the correction terms ends up being non-homogeneous and depends on the leading order terms in a complicated way. As such, we were unable to make analytical progress with this idea.

3. Time-dependent solutions to the Fisher–Stefan model

Fig. 2(a) shows time-dependent solutions of (1)–(3). Here we see that a carefully-chosen initial condition with an appropriate decay in the far field evolves to a travelling wave solution that is visually indistinguishable from (7). To make this point we show the initial condition in green, together some intermediate-time

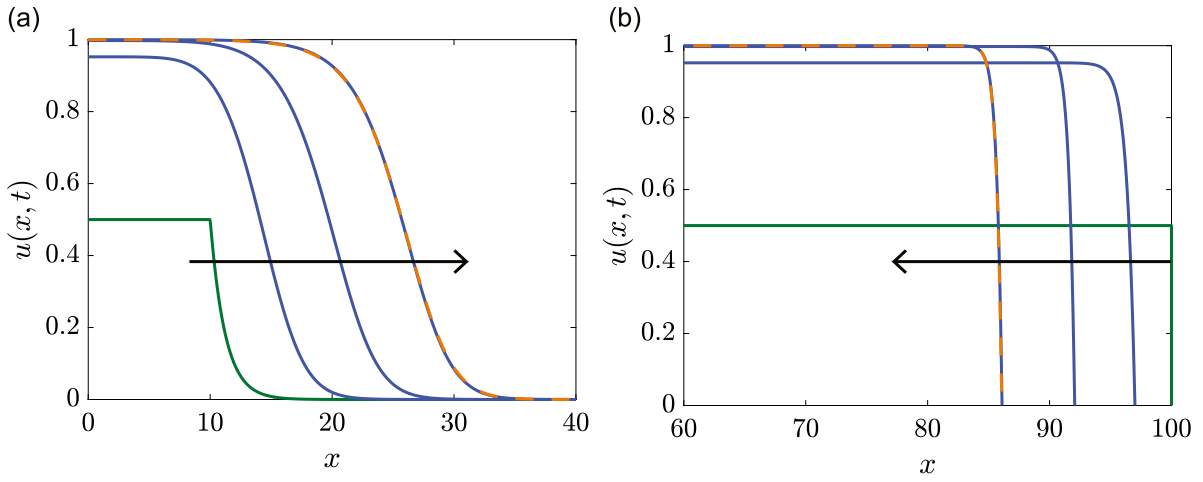

Fig. 2. Time-dependent PDE solutions. (a) Numerical solution of (1)–(3) showing the initial condition (green) as well as intermediate-time solutions at $t = 3$, 6 and 9 (blue). The solution at $t = 9$ is superimposed with (7) (dashed orange). (b) Numerical solution of (4)–(6) showing an initial condition (green) as well as intermediate-time solutions at $t = 3$, 6 and 9 (blue). The solution at $t = 9$ is superimposed with (13)–(14) subject to (16) (dashed orange). (For interpretation of the references to colour in this figure legend, the reader is referred to the web version of this article.)

solutions in blue. The latest solution is superimposed with (7) in dashed orange, confirming that the time-dependent solutions converge to the exact solution reasonably rapidly.

Similar results in Fig. 2(b) show time-dependent solutions of (4)–(6). Here we have used a simple step function for an initial condition, which is shown in green, and have carefully chosen our parameter κ to be $\kappa = c/V^* = -0.906\ldots$. Again we show three intermediate-time solutions in blue at $t = 3$, 6 and 9. The superimposed exact solution (13)–(14) with (16) for $c = -5/\sqrt{6}$ in orange compares extremely well with the numerical solution at $t = 9$, thus demonstrating how quickly the time-dependent solution evolves to the travelling wave solution. Recall that for other values of $-1 < \kappa < 0$, solutions of the full time-dependent problem (4)–(6) will evolve to a different travelling wave profile (that is, it is only the special value $\kappa = -0.906\ldots$ that leads to the exact travelling wave solution discussed here).

Note that we solved (4)–(6) numerically with $\kappa = -0.906\ldots$ using a variety of other initial conditions and in each case the time-dependent solution appeared to evolve to the exact travelling wave profile (13)–(14) for $c = -\sqrt{5}/6$, provided the domain is long enough. As such, we believe the exact travelling wave solution is stable. It would be interesting to prove this stability by writing the solution of (4)–(6) as $u = U(z) + p(z,t)$, $v = V(z) + q(z,t)$, and analysing the leading order problem for p and q. We leave this problem for future research.

4. Conclusion

We present a new interpretation of an exact travelling wave solution of the Fisher–KPP model. The Fisher–KPP model is one of the most well-studied reaction–diffusion equations with applications including wound healing [22–25] and ecological invasion [26,27]. For cell biology applications, the Fisher–KPP model is often used because cells are thought to move randomly, by diffusion, as well as proliferating logistically [24,28]. Experimental observations of moving cell fronts can be described by travelling wave solutions of the Fisher–KPP model [28], or generalisations of the Fisher–KPP model [29]. For the dimensional Fisher–KPP model with diffusivity D, proliferation rate λ and carrying capacity density K, the speed of the travelling wave solution is $c \geq 2\sqrt{\lambda D}$ [4]. In reality, fronts of cells may move at a slower speed or even retreat [10]. One way to deal with this is to write down a more complicated model with more than one

species [30] or with a different source term, like an Allee effect [31]. Even with a single species model that retains a logistic growth term, we can introduce nonlinear degenerate diffusion, leading to the Porous-Fisher model [32], which gives rise to travelling wave solutions with $c \geq \sqrt{\lambda D/2}$ [33,34]. An alternative to all of these modifications is to simply retain Fisher (1) but include a moving boundary as in (4)–(6) [11]. This has appealing features, namely: a sharp moving front, which seems biologically reasonable; retains the classical logistic growth term with an easy to measure λ; allows for solutions of all speeds $c < 2\sqrt{\lambda D}$, including negative speeds [7]. A detailed discussion about how κ could be estimated using data from cell biology experiments is provided in [10].

Despite the apparent simplicity of the Fisher–KPP model, exact solutions are relatively elusive but of high interest since they provide important mathematical insight and can be used as benchmarks for testing numerical methods [35]. It is well-known that the travelling wave solution (7) can be written down exactly for a special wave speed $c = 5/\sqrt{6}$ [18,19]. This special travelling wave is consistent with the usual view that travelling wave solutions of the nondimensional Fisher–KPP have positive speed $c > 2$, whereas solutions with $c < 2$ are normally disregarded on the grounds of being unphysical [4]. In our work we take a different point of view and re-formulate the Fisher–KPP model with a moving boundary, often called the Fisher–Stefan model [7]. The Fisher–Stefan model has several attractive features: (i) travelling wave solutions of the Fisher–Stefan model have a well-defined front without needing to introduce the complication degenerate nonlinear diffusion; (ii) the Fisher–Stefan model gives rise to travelling wave solutions with $-\infty < c < 2$, which is more flexible that the usual Fisher–KPP and Porous-Fisher models since it can be used to model both invasion and retreat; and (iii) the Fisher–Stefan model provides a simple physical interpretation for an exact solution with $c = -5/\sqrt{6}$. This overlooked solution can be expressed exactly using Weierstraß elliptic functions and, as we show numerically, this solution is the long-time limit of our moving boundary problem (4)–(6).

Acknowledgements

SWM would like to thank the Isaac Newton Institute for Mathematical Sciences, Cambridge, for support and hospitality during the programme Complex Analysis: Techniques, Applications and Computations where part of the work on this paper was undertaken. This programme was supported by the EPSRC, United Kingdom grant EP/R014604/1. He is grateful for the generous support of the Simons Foundation, United States who provided further financial support for his visit to the Isaac Newton Institute via a Simons Foundation Fellowship. MJS acknowledges the support of the Australian Research Council via the Discovery Project DP200100177. The authors acknowledge the helpful comments of the anonymous referees.

Appendix A. Supplementary data

Supplementary material related to this article can be found online at https://doi.org/10.1016/j.aml.2020.106918.

References

[1] R.A. Fisher, The wave of advance of advantageous genes, Ann. Eugenics 7 (1937) 355–369.
[2] A.N. Kolmogorov, P.G. Petrovskii, N.S. Piskunov, A study of the diffusion equation with increase in the amount of substance, and its application to a biological problem, Moscow Univ. Math. Bull. 1 (1937) 1–26.
[3] J. Canosa, On a nonlinear diffusion equation describing population growth, IBM J. Res. Dev. 17 (1973) 307–313.
[4] J.D. Murray, Mathematical Biology I: An Introduction, third ed., Springer, New York, 2002.
[5] L. Edelstein-Keshet, Mathematical Models in Biology, SIAM, Philadelphia, 2005.
[6] M. Kot, Elements of Mathematical Ecology, Cambridge University Press, Cambridge, 2003.

[7] M. El-Hachem, S.W. McCue, W. Jin, Y. Du, M.J. Simpson, Revisiting the Fisher–Kolmogorov–Petrovsky–Piskunov equation to interpret the spreading–extinction dichotomy, Proc. R. Soc. Lond. Ser. A Math. Phys. Eng. Sci. 475 (2019) 20190378.
[8] M. El-Hachem, S.W. McCue, M.J. Simpson, A sharp-front moving boundary model for malignant invasion, Physica D 412 (2020) 132639.
[9] M.J. Simpson, Critical length for the spreading-vanishing dichotomy in higher dimensions, ANZIAM J. 62 (2020) 3–17.
[10] M. El-Hachem, S.W. McCue, M.J. Simpson, Invading and receding sharp-fronted travelling waves, Bull. Math. Biol. (2021) arXiv:2008.00662.
[11] Y. Du, Z. Lin, Spreading–vanishing dichotomy in the diffusive logistic model with a free boundary, SIAM J. Math. Anal. 42 (2010) 377–405.
[12] J. Crank, Free and Moving Boundary Problems, Oxford University Press, Oxford, 1987.
[13] S.W. McCue, B. Wu, J.M. Hill, Classical two-phase Stefan problem for spheres, Proc. R. Soc. Lond. Ser. A Math. Phys. Eng. Sci. 464 (2008) 2055–2076.
[14] S.C. Gupta, The Classical Stefan Problem. Basic Concepts, Modelling and Analysis with Quasi-Analytical Solutions and Methods, Elsevier, Amsterdam, 2017.
[15] Y. Du, H. Matano, K. Wang, Regularity and asymptotic behavior of nonlinear Stefan problems, Arch. Ration. Mech. Anal. 212 (2014) 957–1010.
[16] Y. Du, H. Matsuzawa, M. Zhou, Sharp estimate of the spreading speed determined by nonlinear free boundary problems, SIAM J. Math. Anal. 46 (2014) 375–396.
[17] Y. Du, B. Lou, Spreading and vanishing in nonlinear diffusion problems with free boundaries, J. Eur. Math. Soc. 17 (2015) 2673–2724.
[18] P. Kaliappan, An exact solution for travelling waves of $u_t = Du_{xx} + u - u^k$, Physica D 11 (1983) 368–374.
[19] M. Ablowitz, A. Zeppetella, Explicit solutions of Fisher's equation for a special wave speed, Bull. Math. Biol. 41 (1979) 835–840.
[20] M. Abramowitz, I.A. Stegun (Eds.), Handbook of Mathematical Functions with Formulas, Graphs, and Mathematical Tables, Dover Publications, New York, 1965.
[21] P.A. Clarkson, Painlevé Equations — Nonlinear special functions, in: F. Marcellán, W. Van Assche (Eds.), Orthogonal Polynomials and Special Functions, in: Lecture Notes in Mathematics, vol. 1883, Springer, Berlin, Heidelberg, 2006.
[22] S.T. Johnston, J.V. Ross, B.J. Binder, D.L.S. McElwain, P. Haridas, M.J. Simpson, Quantifying the effect of experimental design choices for in vitro scratch assays, J. Theoret. Biol. 400 (2016) 19–31.
[23] B.G. Sengers, C.P. Please, R.O.C. Oreffo, Experimental characterization and computational modelling of two–dimensional cell spreading for skeletal regeneration, J. R. Soc. Interface 4 (2007) 1107–1117.
[24] J.A. Sherratt, J.D. Murray, Models of epidermal wound healing, Proc. R. Soc. Lond.: Ser. B 241 (1990) 29–36.
[25] S.T. Vittadello, S.W. McCue, G. Gunasingh, N.K. Haass, M.J. Simpson, Mathematical models for cell migration with real–time cell cycle dynamics, Biophys. J. 114 (2018) 1241–1253.
[26] J.G. Skellam, Random dispersal in theoretical populations, Biometrika 38 (1951) 196–218.
[27] J. Steele, J. Adams, T. Sluckin, Modelling Paleoindian dispersals, World Archaeol. 30 (1998) 286–305.
[28] P.K. Maini, D.L.S. McElwain, D. Leavesley, Traveling waves in a wound healing assay, Appl. Math. Lett. 17 (2004) 575–580.
[29] D.J. Warne, R.E. Baker, M.J. Simpson, Using experimental data and information criteria to guide model selection for reaction–diffusion problems in mathematical biology, Bull. Math. Biol. 81 (2019) 1760–1804.
[30] K.J. Painter, J.A. Sherratt, Modelling the movement of interacting cell populations, J. Theoret. Biol. 225 (2003) 327–339.
[31] N.T. Fadai, M.J. Simpson, Population dynamics with threshold effects gives rise to a diverse family of Allee effects, Bull. Math. Biol. 82 (2020) 74.
[32] T.P. Witelski, Merging traveling waves for the porous–Fisher's equation, Appl. Math. Lett. 8 (1995) 57–62.
[33] F. Sánchez Garduno, P.K. Maini, An approximation to a sharp type solution of a density–dependent reaction–diffusion equation, Appl. Math. Lett. 7 (1994) 47–51.
[34] J.A. Sherratt, B.P. Marchant, Nonsharp travelling wave fronts in the Fisher equation with degenerate nonlinear diffusion, Appl. Math. Lett. 9 (1996) 33–38.
[35] M.J. Simpson, K.A. Landman, Characterizing and minimizing the operator spit error for Fisher's equation, Appl. Math. Lett. 19 (2006) 604–612.